Analytica Chimica Acta 1006 (2018) 22–32

Contents lists available at ScienceDirect

Analytica Chimica Acta

journal homepage: www.elsevier.com/locate/aca

Entrapment of bimetallic $CoFeSe_2$ nanosphere on functionalized carbon nanofiber for selective and sensitive electrochemical detection of caffeic acid in wine samples

Mani Sakthivel [a], Sukanya Ramaraj [a], Shen-Ming Chen [a, *], Bose Dinesh [b], Hari Vignesh Ramasamy [c], Y.S. Lee [c]

[a] Electroanalysis and Bioelectrochemistry Lab, Department of Chemical Engineering and Biotechnology, National Taipei University of Technology, Taipei 10608, Taiwan
[b] Nano and Bioelectrochemistry Research Laboratory, Department of Chemistry, School of Advanced Sciences, Vellore Institute of Technology University, Vellore, 632 014, Tamil Nadu, India
[c] Faculty of Applied Chemical Engineering, Chonnam National University, Gwangju 500-757, Republic of Korea

HIGHLIGHTS

- A new type of bimetallic $CoFeSe_2$ nanosphere were synthesized and successfully entrapped on the surface of functionalized carbon nanofiber ($CoFeSe_2$/f-CNF) using simple hydrothermal technique.
- $CoFeSe_2$/f-CNF modified electrode exhibits excellent electrocatalytic activity towards the electrochemical detection of caffeic acid (CA).
- The ultra-low detection limit (0.002 μM) of CA were achieved using $CoFeSe_2$/f-CNF modified electrode.
- The excellent electrocatalytic activity of $CoFeSe_2$/f-CNF facilitate the detection of CA in wine.

GRAPHICAL ABSTRACT

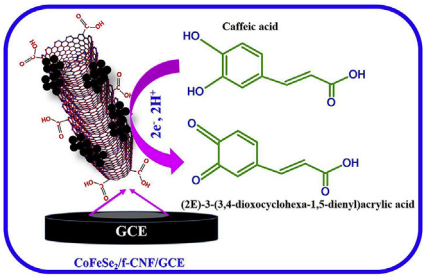

ARTICLE INFO

Article history:
Received 8 September 2017
Received in revised form
23 December 2017
Accepted 27 December 2017
Available online 6 January 2018

Keywords:
Metal chalcogenide
Metal selenide
Hydrothermal synthesis
$CoFeSe_2$
Electrochemical sensor
Caffeic acid

ABSTRACT

The ever-increasing requirement of an electrochemical sensor in various paramedical and industrial applications, the recent research is motivated to fabricate a new type of electrode material with unique electrochemical properties for quantitative detection of various target analytes. Recently, the metal diselenides have been interested in a broad range of electrochemical applications due to their interesting electrocatalytic performances. Despite the metal diselenides have been widely focused on hydrogen evolution reaction (HER) and oxygen reduction reaction (ORR), it is not much focused on electrochemical sensor. For the first time, the bimetallic cobalt-iron diselenide nanosphere entrapped functionalized carbon nanofiber ($CoFeSe_2$/f-CNF) composite have been synthesized by using simple hydrothermal synthesis and used as an electrode material for efficient electrochemical detection of caffeic acid (CA). The functionalization of CNF and the formation of $CoFeSe_2$/f-CNF nanocomposite have been successfully scrutinized by using Fourier transform infrared spectroscopy, Raman spectroscopy, X-ray powder diffraction, transmission electron microscopy and scanning electron microscopy, energy dispersive X-ray spectroscopy, and X-ray photoelectron spectroscopy. In addition, the electrochemical properties of

* Corresponding author.
E-mail address: smchen78@ms15.hinet.net (S.-M. Chen).

https://doi.org/10.1016/j.aca.2017.12.044

$CoFeSe_2$/f-CNF modified glassy carbon electrode (GCE) towards CA sensing were investigated by using cyclic voltammetry, differential pulse voltammetry and electrochemical impedance spectroscopy. As the result of the electrochemical studies, the developed $CoFeSe_2$/f-CNF/GCE sensor exhibits very low detection limit (0.002 μM) and better sensitivity (2.04 μA μM^{-1} cm^{-2}) of CA. And also, $CoFeSe_2$/f-CNF/GCE sensor shows the feasible detection of CA in red wine samples, it reveals the excellent practicability of $CoFeSe_2$/f-CNF/GCE.

1. Introduction

As a new metal chalcogenide, metal diselenides have been received enormous interest in recent research owing to their excellent physical and electrochemical properties [1–3]. In general, the Se based metal chalcogenides exhibit enhanced electrochemical activities than S based metal chalcogenides because of the higher metallic property of Se [4]. Herein, Se is the more adjacent chemical element to O and S in the sixth main group of the periodic table and exhibiting identical properties with one another. Recently, many metal diselenides MSe_2 (M = Fe, Co, Mo, Ni, Cu and Mn etc.) have been synthesized and applied as an active electrode material in numerous electrochemical applications including solar cells, batteries, supercapacitors, fuel cells, hydrogen evolution reactions (HER), oxygen reduction reactions (ORR) and especially in electrochemical sensors [5–10]. Among these MSe_2, many research articles have been published on $FeSe_2$ and $CoSe_2$ due to their excellent electrical conductivity, enlarged surface area, shortened diffusion length for both ion and electron, high specific capacitance, cycling stability, low charge transfer resistance and substantial electrocatalytic activity, etc., [11–15]. For instance, *Huaqing Xiao* et al., reported the synthesis of lamellar structured $CoSe_2$ nanosheets and used as an efficient catalyst for hydrogen evolution reaction [16] and *Feipeng Zhao* et al., prepared ultra-small $FeSe_2$ nanoparticle for enhancing sodium ion storage performance [17]. Interestingly, the low spin configuration of a 3d electron in cofacilitate the high metallic property to $CoSe_2$, which can increase the charge transfer along the catalytic process [16]. At the same time, the doping of Fe effectively improved the catalytic activity of $CoSe_2$, because of the small d% difference between Fe (39.5) and Co (39.7) offers higher binding ability as well as enhance the high surface area and efficient electron transfer [18]. Hence, the synergistic effect between Fe and $CoSe_2$ could beneficially enhance the electrocatalytic activity of Fe/$CoSe_2$ alloy. Although the electrocatalytic behavior of $FeSe_2$, $CoSe_2$, and Fe/$CoSe_2$ alloy have been well studied for aforementioned applications, still the Fe/$CoSe_2$ alloy has not been used as an electrode material for electrochemical sensor. Encouraged by these above mentioned studies, $CoFeSe_2$ anchored functionalized carbon nanofiber (f-CNF) was prepared and applied as an active electrode material towards the sensing of caffeic acid (CA). In general, the carbon-based nanomaterials such as carbon nanotube (CNT), carbon nanofiber (CNF), graphene, carbon nanosphere and activated carbon have been considered as promising supportive and active materials due to their high surface area, outstanding electrical conductivity, high electrocatalytic activity and more stability, etc. [19–21]. Recently, carbon nanofiber (CNF) has been developed as a promising electrode material in numerous applications owing to the larger surface to volume ratio than CNT [22], interesting cylindrical nanostructure with stacking arrangement of graphene sheets and more edge plane defects on outer wall offer efficient electron transfer [23]. Mainly, the functionalized CNF (f-CNF) exhibits high solubility and high electrocatalytic activity than pristine CNF because of more anchoring sites and surface reactive carboxylic acid, hydroxyl and carbonyl groups on its open end/side walls [24]. Hence, the integration of f-CNF could effectively enhance the electrochemical properties of $CoFeSe_2$ towards the electrochemical detection of CA.

CA is a well-known phenolic acid found in various fruits and vegetables including broccoli, citrus fruit, tea, coffee, and wines [25]. The molecular structure of CA contains two hydroxyl groups which are a significant contribution to unique antioxidant properties of CA. Interestingly, the CA exhibits numerous pharmaceutical activities such as antiallergic, antibacterial, antitumor effect and reduce inflammation [26]. The intake of CA contains foods are recommended to be included in diet habits and new dietary supplements. For instance, drinking of CA includes coffee and wines is significantly prevent the neurodegeneration and brain injury. Moreover, the HIV replication also can stop by CA due to its potential pharmaceutical activities [27]. Thus, the quantitative detection of CA is more beneficial for healthcare and qualitative analysis. Nowadays, different techniques have been developed for the determination of CA in wine such as electrophoresis [28], electron-spray ionization mass spectroscopy [29] and High-pressure liquid chromatography [30]. These aforementioned methods have some difficulties including high cost, require expensive instrumental set up and more time-consuming process. In order to overcome such difficulties, the electrochemical method has been recently preferred due to low-cost, easy sample preparation and sensitive detection even at low concentration of target analyte [31].

The present study is the first attempt to prepare a $CoFeSe_2$/f-CNF nanocomposite by a hydrothermal method and applied as a useful electrode material for sensitive electrochemical detection of CA. Numerous analytical techniques were performed to scrutinize the structural changes and crystalline properties of the $CoFeSe_2$/f-CNF nanocomposite. Remarkably, $CoFeSe_2$/f-CNF/GCE is found with high electrocatalytic activity towards the oxidation of CA than bare GCE, f-CNF/GCE and $CoFeSe_2$/GCE . The nanostructured $CoFeSe_2$/f-CNF/GCE shows an outstanding performance towards the detection of CA in terms of wide linear range, excellent sensitivity (2.04 μA μM^{-1} cm^{-2}) and ultra-low detection limit of 2.0 nM. In addition, the present sensor has the advantages of reliable stability, and selectivity. The real sample analysis also stated that the feasible practicability of $CoFeSe_2$/f-CNF/GCE towards the sensing of CA in wine sample.

2. Experiment section

2.1. Materials and reagents

The $Co(NO_3)_2$. $6H_2O$, N_2H_4. H_2O purchased from ACROS chemicals. $FeCl_3$. $6H_2O$, Na_2SeO_3, caffeic acid and carbon nanofiber (CNF, D × L = 100 nm × 20–200 μM, average pore volume = 0.075 cm^3/g) were purchased from Sigma Aldrich. The supporting electrolyte 0.05 M phosphate buffer solution (PBS) (pH 7) was prepared by mixing of 0.05 M Na_2HPO_4 and NaH_2PO_4, and the pH of the PBS was

varied by adding NaOH/H_2SO_4. All chemicals reagents were of analytical grade and were used without further purification.

2.2. Functionalized of carbon nanofiber (f-CNF)

In this functionalization process, 1 g of CNF was added to the 40 mL of HNO_3/H_2SO_4 (1:3) acid mixture at 50 C for 8 h with continuous magnetic stirring. Herein, the addition of H_2SO_4 was used to make defect sites and HNO_3 for generating the oxygen functional groups (carboxylic acid, hydroxyl, and carbonyl groups). After the continuous stirring, the resultant functionalized CNF solution was centrifuged and washed with an obvious amount of DD water until the pH value attains around 7. Finally, the resultant f-CNF was dried in vacuum oven for overnight [24].

2.3. Hydrothermal synthesis of $CoFeSe_2$/f-CNF nanocomposite

The $CoFeSe_2$/f-CNF nanocomposite was prepared in hydrothermal technique by the following procedure. In this experiment, the as-prepared f-CNF (5 mg/mL) was dispersed in 20 mL of water by ultrasonication for 15 min. Then, the f-CNF solution was transferred to stirring with the further additions of 0.02 M $FeCl_3$. $6H_2O$, 0.02 M $Co(NO_3)_2$. $6H_2O$ and 0.04 M Na_2SeO_3 powder were mixed into the above solution under vigorous magnetic stirring. After 10 min stirring, 2 mL hydrazine hydrate was added to the above mixture and observed the formation of black color precipitation by continuous stirring for 30 min. The resultant solution was transferred into 50 mL Teflon equipped autoclave and subjected to 180 C for 12 hrs in the hot air oven. After heating, the autoclave was allowed to cool at room temperature. The resulting black color precipitation was washed with ethanol and water, then dried in hot air oven at 45 C for a whole night. The followed synthesis process is clearly illustrated in Scheme 1.

2.4. Characterizations

The crystalline properties of $CoFeSe_2$/f-CNF nanocomposite were analyzed by using XRD (XPERT-3 diffract meter with Cu Kα radiation (K = 1.54 Å)). Fourier transform infrared spectroscopy (FT-IR) measurement was recorded using JASCO FT/IR-6600. Raman spectroscopy was a recorded by using WITech CRM200 confocal microscopy Raman system with a 488 NM laser. The surface morphology of $CoFeSe_2$ and $CoFeSe_2$/f-CNF nanocomposite were recorded by using TEM (JEOL 2100F). Scanning Electron Microscopy (SEM) was performed by using Hitachi S-3000 H electron microscope. Energy dispersive X-ray (EDX) spectrum was recorded using HORIBA EMAX X-ACT that was attached with Hitachi S-3000 H scanning electron microscope. X-ray photoelectron spectroscopy (XPS) also has been registered by using Thermo scientific multi-lab 2000. Electrochemical impedance spectroscopy (EIS) has been recorded by using IM6ex ZAHNER impedance measurement unit. The electrochemical behavior of $CoFeSe_2$/f-CNF nanocomposite has been registered by using CV (CHI611A electrochemical analyzer) and, DPV (CHI900 electrochemical analyzer). In this all electrochemical studies, the conventional three-electrode system where glassy carbon electrode (GCE) was used as a working electrode, a saturated Ag/AgCl electrode as a reference electrode and a platinum wire as the auxiliary electrode. All measurements were carried out at room temperature.

2.5. Fabrication of $CoFeSe_2$/f-CNF nanocomposite modified GCE

The $CoFeSe_2$/f-CNF dispersion was prepared by dispersing of 1 mg $CoFeSe_2$/f-CNF in 1 mL ethanol and sonicated for 15 min. Subsequently, the 6 μL of the $CoFeSe_2$/f-CNF suspension was coated on GCE surface and dried in an oven at 45 C. After that, the dried GCE was gently rinsed with DD water to remove the loosely aggregated materials on the GCE surface. Finally, the obtained $CoFeSe_2$/f-CNF modified GCE was used for further electrochemical studies.

3. Results and discussion

3.1. Characterizations of $CoFeSe_2$/f-CNF nanocomposite

The morphological characteristic of $CoFeSe_2$/f-CNF has been clearly investigated by using TEM and displayed in Fig. 1. The sphere-like the structure of $CoFeSe_2$ with uniform size of about ~7 nm can be observed in Fig. 1 (A, B). The HRTEM image of $CoFeSe_2$ nanospheres (Fig. 1C) shows the lattice fringes with a d spacing of

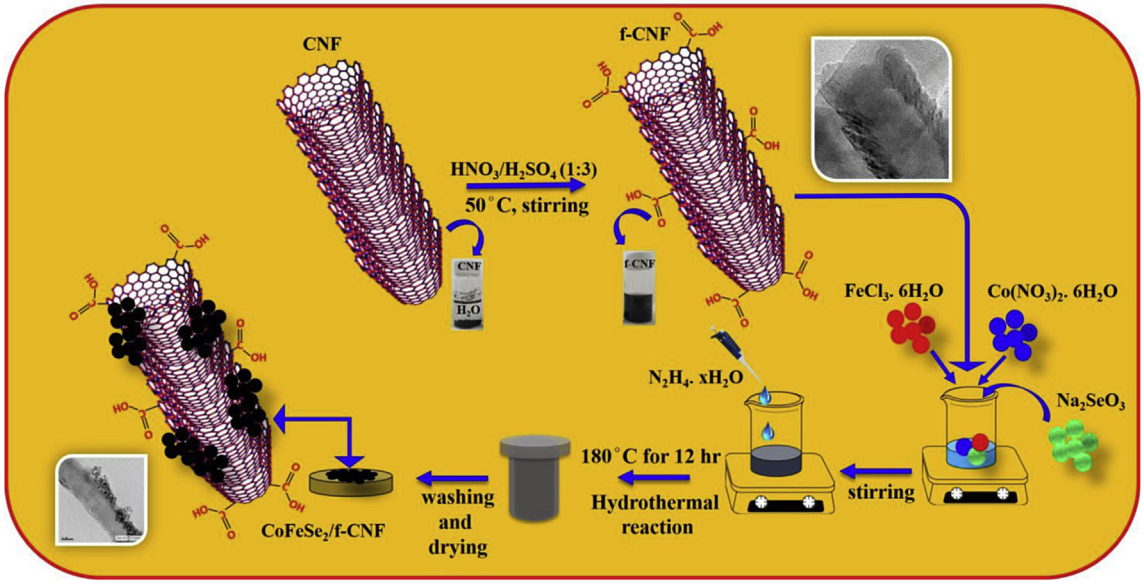

Scheme: 1. Schematic illustration for the synthesis of $CoFeSe_2$/f-CNF nanocomposite.

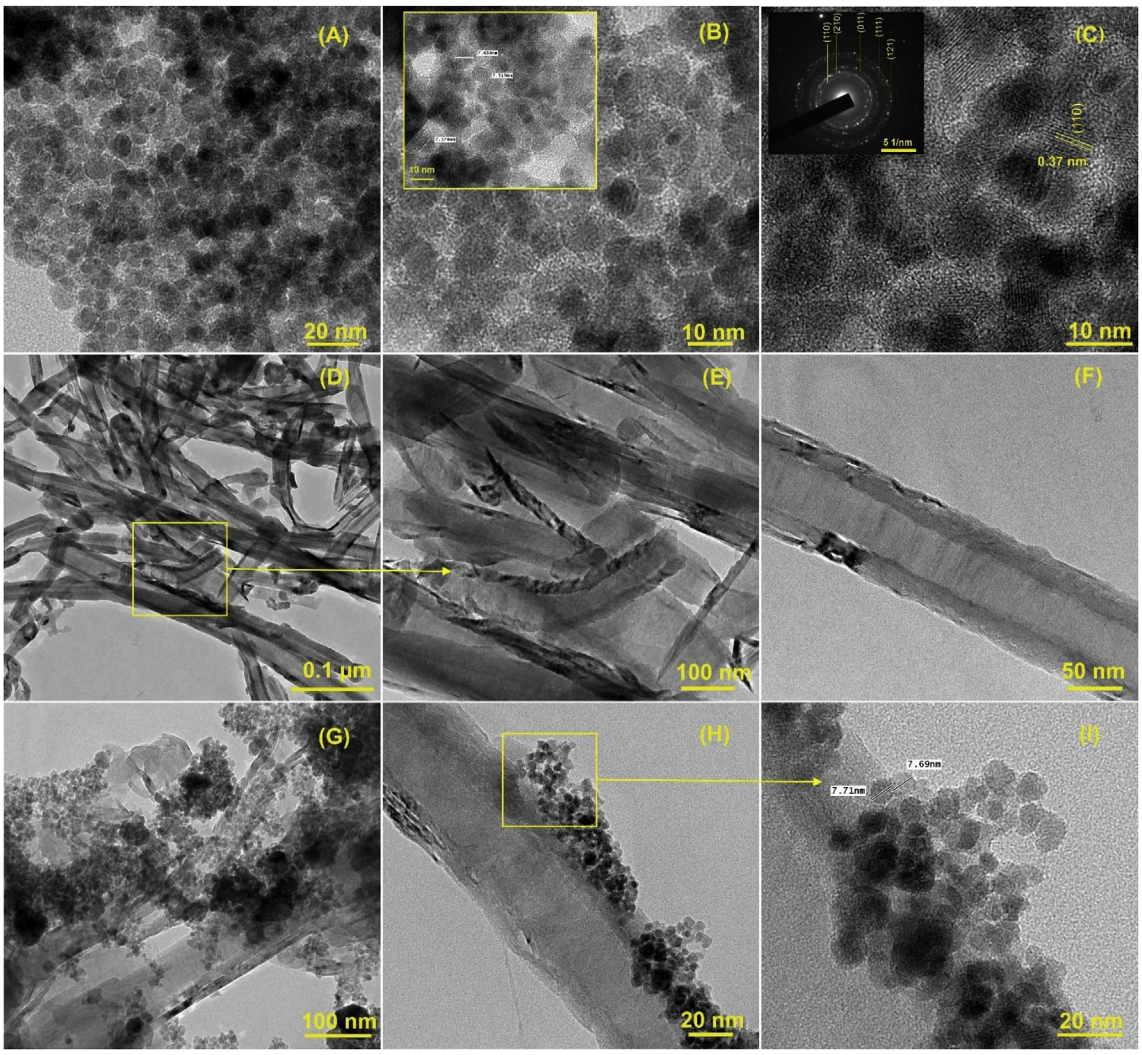

Fig. 1. Different magnified TEM images of (A-C) $CoFeSe_2$, (D-F) f-CNF and (G-I) $CoFeSe_2$/f-CNF nanocomposite.

0.37 nm for corresponding lattice plane (110). And also, the selected area electron diffraction (SAED) pattern of $CoFeSe_2$ is shown in Fig. 1C (inset). The more bright spots on each fringe of SAED pattern reveals the polycrystalline nature of $CoFeSe_2$. The first five fringes in SAED pattern are intensely assigned to the (110), (210), (011), (111) and (121) planes, which is good agreement with XRD pattern of $CoFeSe_2$. In addition, the stacking arrangement of graphene-like nanosheets is observed which may due to the unzipping of f-CNF, and the images are shown in Fig. 1D-F. Especially, Fig. 1E shows the f-CNF with a shortened length and an open end, which reveals the functionalization of CNF. Afterward, the integration of $CoFeSe_2$ on f-CNF was successfully examined by observing the TEM images (Fig. 1 (G–H)). $CoFeSe_2$ nanospheres with an average diameter of < 5 nm are uniformly distributed on the surface of f-CNF, whereas the diameter of the particle in composite (Fig. 1I) is almost identical to $CoFeSe_2$ nanospheres (Fig. 1B (inset)).

Further characterization techniques were followed to confirm the formation of $CoFeSe_2$. Fig. S1(A) shows the EDX spectra of $CoFeSe_2$ with resultant sharp peaks of Co, Fe and Se elements and the considerable quantitative weight percentage were recorded for Co, Fe and Se elements of about 1.15%, 0.71% and 0.12% respectively and its corresponding bar diagram is shown in Fig. S1(B). Fig. S1(C) shows the SEM images of $CoFeSe_2$, which shows the aggregated nanosphere of $CoFeSe_2$, the corresponding elemental mapping for Co, Fe and Se elements are shown in Fig. S1(D-F), which evidently confirms the uniform distribution of Co, Fe, and Se_2, where these all major elements were represented in different colors.

The functionalization of CNF and the formation of $CoFeSe_2$/f-CNF nanocomposite are confirmed by using FT-IR analysis. The characteristic peaks in the FT-IR spectra of f-CNF (Fig. 2A (a)) at 1720, 1047 and 1227 cm^{-1} correspond to the oxygen functional groups C=O, C-OH and C-O-C respectively [24]. For the comparison, Fig. S2 shows the FT-IR spectrum of unfunctionalized CNF with weak observed peaks. Thus, the functionalization of CNF was successfully scrutinized. Fig. 2A (b) shows the FTIR spectrum of the $CoFeSe_2$ with corresponding peaks at 910.39, 1042.97, 1088.17, 1648.02 and 3304.19 cm^{-1} corresponds to Fe and Co complex bonding with Se [16,32]. The formation of the nanocomposite was apparently confirmed by observing the FT-IR spectra (Fig. 2A (c)), which consists the FT-IR peaks of both f-CNF and $CoFeSe_2$.

The Raman spectra also evidently confirm the functionalization of CNF through the variation in the relative intensity of D band and G band. Fig. S3 shows the Raman spectra of both CNF and F-CNF with two well-defined D and G band at 1368 cm^{-1} and 1617 cm^{-1} respectively. In general, the D band attributed due to disordered (sp^2 bonded sites) nature of the graphitic structure and G band is

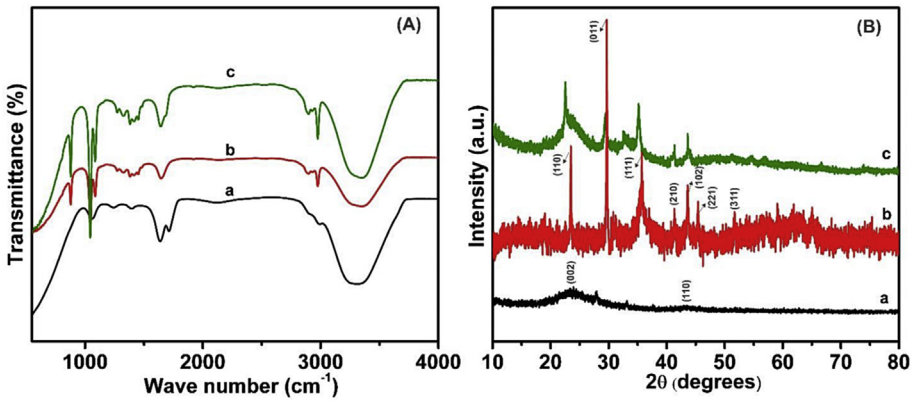

Fig. 2. FTIR spectra and XRD pattern of (a) f-CNF, (b) $CoFeSe_2$ and (c) $CoFeSe_2$/f-CNF nanocomposite.

due to the C-C stretching in the graphitic material. The increasing intensitive of D band in F-CNF due to the formation of defect on the surface of CNF as the result of functionalization process. The intensity ratio of the D band to the G band (I_D/I_G) is often used to estimate the defect concentration in carbon materials. The I_D/I_G ratio of CNF is 0.95 lower than that value 1.01 of F-CNF are confirming the functionalization process.

The XRD pattern was recorded for f-CNF, $CoFeSe_2$ and $CoFeSe_2$/f-CNF as shown in Fig. 2B. Fig. 2B (a) shows the most intense diffraction peaks of f-CNF at 23.74 and 42.96 with corresponding lattice planes (002) and (110) respectively. The observed carbon peaks are greatly assigned to the hexagonal carbon crystal face with standard data of CNF (JCPDS 75-1621). Fig. 2B (b) shows the major diffraction peaks of $CoFeSe_2$ at 23.4 , 29.67 , 35.77 , 41.28 , 43.72 , 45.25 and 52.3 with corresponding lattice planes are (110), (011), (111), (210), (102), (221) and (311) respectively, which are similar to the XRD pattern of orthorhombic phase $FeSe_2$ (JCPDS card no. 21 -0432) and orthorhombic phase $CoSe_2$ (JCPDS No. 09-234) [33,34]. In addition, the sharp diffraction peaks are representing the high crystalline purity of $CoFeSe_2$. Hence, the followed hydrothermal technique can be considered as a promising way to prepare the $CoFeSe_2$ with uniform size and shape. Fig. 2B (c) shows the diffraction peaks of both $CoFeSe_2$ and f-CNF, which confirms the formation of $CoFeSe_2$/f-CNF nanocomposite.

The chemical and surface electronic state of the element in $CoFeSe_2$ were successfully scrutinized by using XPS analysis and presented in Fig. 3. Fig. 3A shows the survey spectrum of $CoFeSe_2$ with significant characteristic peaks at 792.9, 721.08, 534.6, 287.4 and 56.9 eV for Co 2p, Fe 2p, O 1s, C 1s and Se 3d respectively. The C (as the reference) and O elements were recorded from the surface adsorption due to the exposure of air. As a result, the reported $CoFeSe_2$ nanosphere contains only the Fe, Co and Se elements in near-surface range. Fig. 3B-D show the high-resolution XPS spectra of Fe 2p, Co 2p, and Se 3d respectively. The XPS spectra of Fe 2p illustrates the peak at 710.4 and 712.6 eV for Fe^{2+} $2p_{3/2}$ and Fe^{3+} $2p_{3/2}$ states respectively. The transition peaks on higher energy state at 724.29 and 726.26 eV are strongly assigned to Fe $2p_{1/2}$ state. The two satellite peaks at 719.15 and 733.34 eV are strongly indicate the divalent state of Fe in $CoFeSe_2$. In addition, the XPS spectra of Co 2p contains the sharp peaks at 780.53 eV is due to the Co $2p_{3/2}$, which is containing the corresponding Co^{3+} $2p_{3/2}$ and Co^{2+} $2p_{3/2}$ states at 779.93 and 781.38 eV respectively. Herein, the Co^{2+} originate with a strong shake-up satellite peaks at 786.06 eV, while Co^{3+} did not show any satellite peaks. The peaks at 796.37 eV are represented the Co $2p_{1/2}$ state with the satellite peaks at 803.5 eV also strongly confirm the existence of Co (II). The metal selenide bond is evidently identified through the observed peaks at 59.43 and 54.85 eV for Se $3d_{3/2}$ and Se $3d_{5/2}$. Thus, XPS analysis confirms that the formation of $CoFeSe_2$ nanosphere and the distribution of Co, Fe, and Se with corresponding electronic states, which is good agreement with other previously reported literature [35].

EIS is a promising technique to analyze the interfacial properties between the electrode and electrolyte [36]. Hence, EIS was performed to the fabricated $CoFeSe_2$/f-CNF/GCE subjected and compared the obtained result to other modified electrodes including bare GCE, $CoFeSe_2$/GCE and f-CNF/GCE. Fig. 4A shows the EIS curve of bare GCE, $CoFeSe_2$/GCE, f-CNF/GCE and $CoFeSe_2$/f-CNF/GCE in 5 mM of $[Fe(CN)_6]^{3-/4-}$ contain 0.1 M of KCl in the frequency range from 0.1 Hz to 100 kHz at AC applied the potential of 10 mV. The obtained results were reported in the form of Nyquist plots. The impedance data were fitted to the Randles circuit shown in the inset of Fig. 4A, where R_{ct} is charge transfer resistance, R_s is electrolyte resistance, Z_w is Warburg impedance and C_{dl} is double layer capacitance. In EIS curve, the diameter of the semicircle is equal to the R_{ct} value which is related to the electron transfer kinetics of the redox probe at the electrode/electrolyte interface. The R_{ct} values of bare GCE, $CoFeSe_2$/GCE, f-CNF/GCE and f-CNF/$CoFeSe_2$/GCE were calculated about 449.13, 406.13, 3.97 and 3.73 Ω respectively. As a result, the integration of f-CNF is actually reduced the R_{ct} of $CoFeSe_2$. These results demonstrate that $CoFeSe_2$/f-CNFs ensures good electrical contact between the electrode and electrolyte and presence of f-CNFs made the charge transfer easier.

In order to analyze the electron transfer behavior of the modified electrodes, CV experiment was performed for bare GCE, $CoFeSe_2$, f-CNF and $CoFeSe_2$/f-CNF/GCE in 5 mM of $[Fe(CN)6]^{3-/4-}$ contain 0.1 M of KCl at 50 mV s^{-1} as shown in Fig. 4B. In result, $CoFeSe_2$/f-CNF/GCE exhibit higher oxidation and reduction response with a smaller peak to peak separation value of about 0.08 V, while the peak to peak separation value was recorded for GCE, $CoFeSe_2$, f-CNF of about 0.142, 0.104 and 0.09 V respectively. The obtained results coincide with the EIS results. The lowest Peak to peak separation and highest peak current observed is due to the fast electron transfer kinetics at $CoFeSe_2$/f-CNF modified electrode.

3.2. Electrocatalytic activity of $CoFeSe_2$/f-CNF/GCE towards the sensing of CA

Fig. 5A shows cyclic voltammograms (CVs) of GCE (a), f-CNFs/GCE (b), $CoFeSe_2$/GCE and $CoFeSe_2$/f-CNFs/GCE (d) in PBS (pH 7) at a scan rate of 50 mV s^{-1}. The CV of bare GCE shows an anodic peak at 0.45 V with a less prominent cathodic peak at about -0.01 V corresponding to the oxidation and reduction of a phenolic group of caffeic acid. The very low current magnitudes of 1.2 μA for I_{pa} and 0.2 μA for I_{pc} arise due to its large R_{ct} value. The CV of $CoFeSe_2$/f-CNF

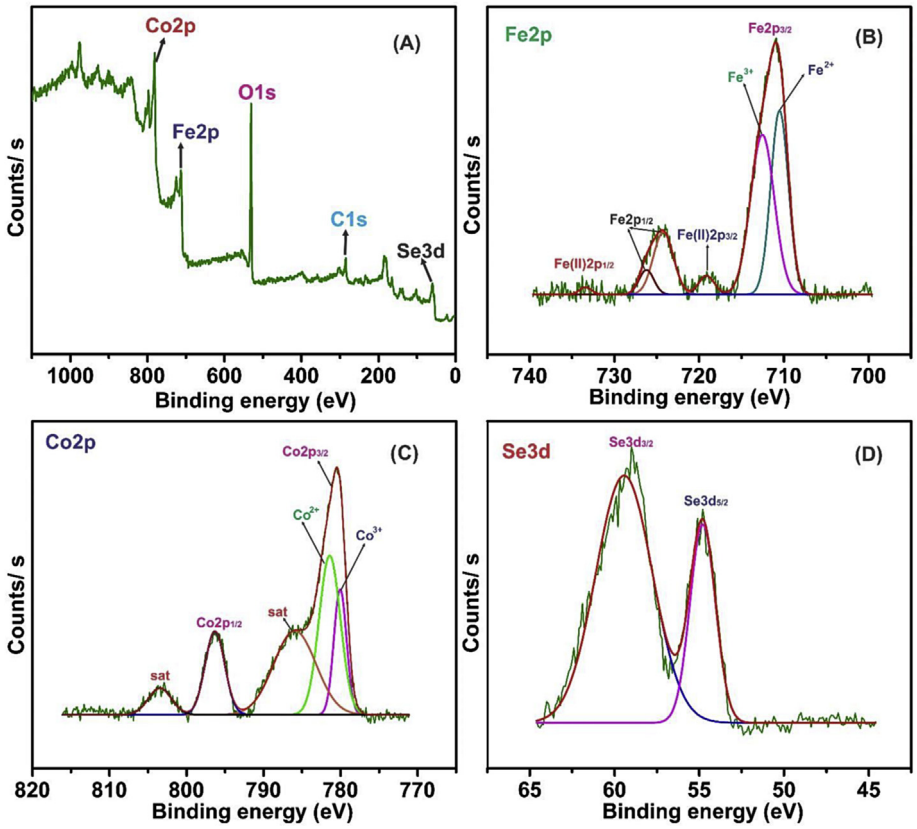

Fig. 3. (A) The full XPS scan and high resolution of $CoFeSe_2$, XPS spectra of (B) Fe 2p, (C) Co 2p and (D) Se 3d.

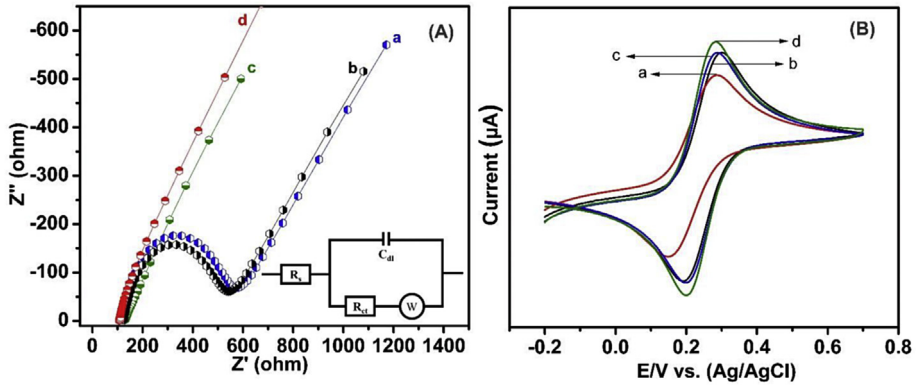

Fig. 4. (A) EIS curve of bare (a) GCE, (b) $CoFeSe_2$/GCE, (c) f-CNF/GCE and (d) $CoFeSe_2$/f-CNF/GCE in 5 mM of $[Fe(CN)6]^{3-/4-}$ contain 0.1 M of KCl in the frequency range from 0.1 Hz to 100 kHz. Inset: Randles circuit model. (B) CV response of (a) bare GCE (b) $CoFeSe_2$/GCE (c) f-CNF/GCE and (d) $CoFeSe_2$/f-CNF/GCE in 5 mM of $[Fe(CN)6]^{3-/4-}$ contain 0.1 M of KCl at scan rate of 50 mV s^{-1}.

modified electrode shows well-defined redox peaks (E_{pa} at 0.22 and E_{pc} at 0.2 V) for the quinone/hydroquinone redox couple of caffeic acid with a peak to peak separation value of (ΔE_p) 20 mV corresponding to a two-electron reversible process. The peak current magnitudes are also found to be substantially improved compared to those of bare GCE, and their ratio is close to unity as expected for a reversible process. In order to bring out the role of f-CNFs and $CoFeSe_2$ in the oxidation of caffeic acid, the CVs have been obtained with $CoFeSe_2$/GCE and f-CNFs/GCE as well. The CV of $CoFeSe_2$/GCE does not show well defined characteristic electrochemical redox process corresponding to the quinone/hydroquinone group of caffeic acid suggesting that the electron transfer is not facile. This is perhaps due to the poor conductivity of the electrode. On the other hand, the CV of f-CNF/GCE shows a pair of redox peaks at E_{pa} and E_{pc} at 0.23 V and 0.19 mV respectively with a ΔE_p of 40 mV indicating that the redox process can also be observed at this modified electrode. However, a comparison of ΔE_p and the ratio of peak currents between f-CNF/GCE and $CoFeSe_2$/f-CNFs/GCE clearly suggest that the electron transfer rather faster at the latter electrode. The oxidation of CA to orthoquinone derivative, while the consequent reduction peak is due to the decrease of the ortho-quinone derivative to CA *via* two electron transfer process, which is clearly demonstrated in Scheme 2.

Fig. 5B shows the CV response of $CoFeSe_2$/f-CNF/GCE for varying

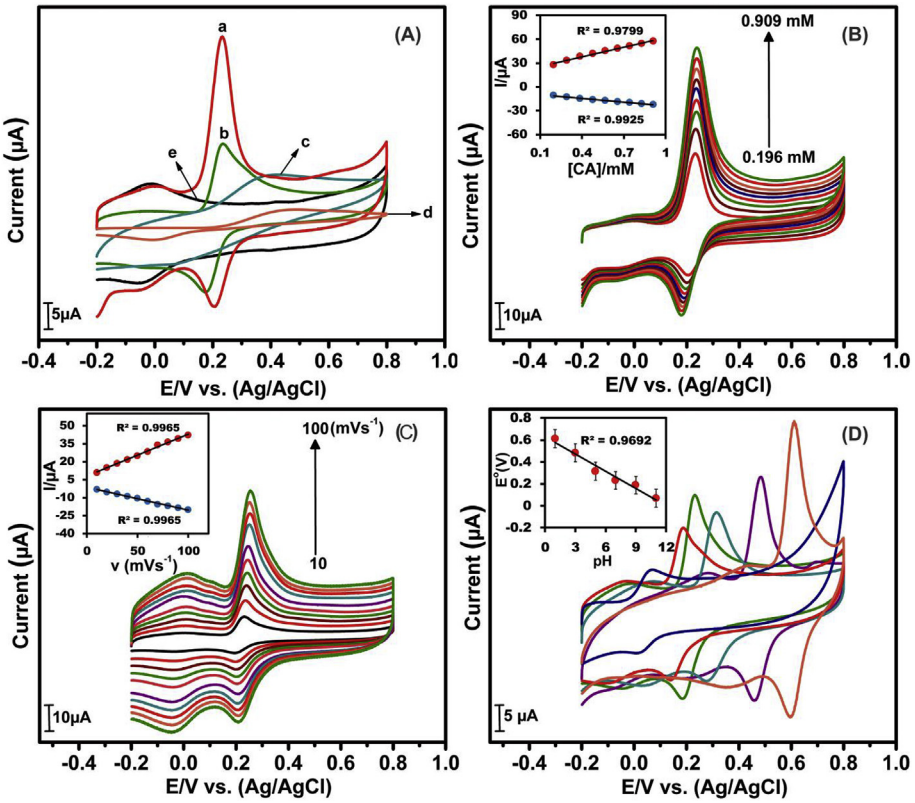

Fig. 5. (A) CV profile of (a) $CoFeSe_2$/f-CNF/GCE and (b) f-CNF/GCE (c) $CoFeSe_2$/GCE and (d) bare GCE for presence of CA (0.196 mM) (e) $CoFeSe_2$/f-CNF/GCE without presence of CA in N_2 saturated PBS (pH 7) at scan rate of 50 mVs^{-1}. (B) CV curve of $CoFeSe_2$/f-CNF/GCE by varying the concentration of CA (0.196–0.909 mM). (C) CV profile of f-CNF/$FeCoSe_2$ modified GCE with the presence of CA in N_2 saturated PBS (pH 7) by varying scan rate from (10–100 mV s^{-1}) respectively. (D) CV profile of $CoFeSe_2$/f-CNF/GCE with the presence of CA in N_2 saturated PBS (pH 1 to pH 11) at a scan rate of 50 mVs^{-1}.

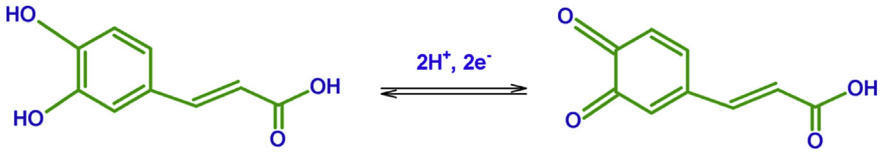

Scheme: 2. Possible electrochemical redox mechanisms of caffeic acid.

the concentration of CA from 0.196 mM to 0.909 mM in N_2 saturated 0.05 M PBS (pH 7) at a scan rate of about 50 mV s^{-1}. The enhanced electrocatalytic activity of $CoFeSe_2$/f-CNF/GCE can be understood by observing the linear increment in redox current for the linear addition of CA. The linear calibration plot for both oxidation and reduction peak current vs concentration of CA is shown in Fig. 3B (inset) with resultant linear regression equation of I_{pa} (μA) = 40.21 mM + 21.90 ($R^2 = 0.9799$) and I_{pc} (μA) = - 16.094 mM−8.008 ($R^2 = 0.9925$) respectively. It clearly confirms that the reported $CoFeSe_2$/f-CNF/GCE is a promising electrode material for effective electrochemical detection of CA without any fouling effect. The redox response of CA at $CoFeSe_2$/f-CNF/GCE is studied by varying the scan rate. Fig. 5C shows the CV response of $CoFeSe_2$/f-CNF/GCE for CA (0.196 mM) in N_2 saturated 0.05 M PBS (pH 7) by changing the scan rate from 10 to 100 mV s^{-1}. By changing scan rate, the relative anodic peak potential is slightly shifted to the positive side. Fig. 5C (inset) shows the corresponding linear calibration plot for oxidation and reduction peak current *vs.* scan rate with i_{pa} (μA) = 0.349 μA/mV s^{-1} + 7.96 ($R^2 = 0.9965$) and i_{pc} (μA) = - 0.1929 μA/mV s^{-1}–1.27 ($R^2 = 0.9965$) respectively, which reveals that the overall redox process of CA at $CoFeSe_2$/f-CNF/GCE is a typical surface controlled process. In order to study the influence of pH for the oxidation of CA (0.196 mM) at $CoFeSe_2$/f-CNF/GCE, pH of the PBS was varied from 1 to 11 at a scan rate of 50 mV s^{-1}, and the obtained result is shown in Fig. 5D. The results show that the formal potential of the redox couple responsible for the quinone/hydroquinone group of oxidized CA which shifts negatively with an increase in pH. A plot of formal potential against pH is linear as exemplified in the inset to Fig. 5B, which indicates that the electron transfer between the $CoFeSe_2$/f-CNF/GCE and the analyte is accompanied by proton transfer. The obtained slope value of 54 mV/pH is closer to that of the Nernstian theoretical value of 59 mV/pH for a reversible equal electron transfer coupled with a proton.

The DPV technique is known as a promising method to scrutinize the electrochemical activity of modified electrodes and calculate the necessary electrochemical parameters such as a limit of detection (LOD), linear range and sensitivity of target analyte. Hence, the DPV was performed for $CoFeSe_2$/f-CNF/GCE with the direct addition of CA concentration from 0.01 to 263.96 μM in N_2 saturated 0.05 M PBS (pH 7), where the resultant linear oxidation peak current response is shown in Fig. 6A. The relationship

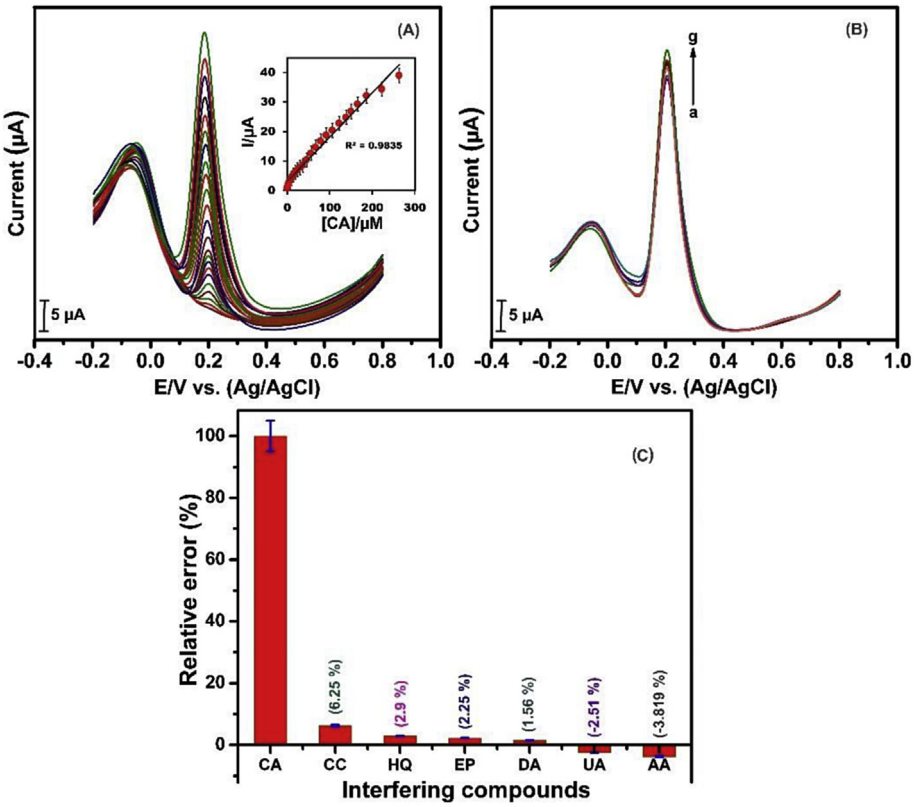

Fig. 6. DPV response of $CoFeSe_2$/f-CNF/GCE for linear addition of CA (0.29–263.96 μM) in N_2 saturated PBS (pH 7). DPV response for interference study for the addition of (c) CA (250 μM) and 50-fold higher concentration of (a) AA, (b) UA, (d) DA, (e) EP, (f) HQ and (g) CC. (C) The corresponding bar diagram of interference study.

between the concentration of CA and obtained oxidation peak current is clearly identified using the linear equation plot as shown in the inset of Fig. 6A. Herein, the linear regression equation was calculated as Ipa (μA) = 0.1496 μM + 3.1625 ($R^2 = 0.9835$). Thus, The limit of detection (LOD) has been calculated using the standard equation, $LOD = 3\sigma/S$, where σ is the standard deviation of the blank signal and S is the slope. As a result, the detection limit is calculated to be 0.002 μM, and the sensitivity of the proposed sensor has been calculated to be 2.04 μA μM^{-1} cm^{-2}. The obtained analytical parameters such as linear range, sensitivity, and detection limit of CA at $CoFeSe_2$/f-CNF/GCE has been compared with previously reported CA sensors as shown in Table 1. From this comparison table, we identified that $CoFeSe_2$/f-CNF/GCE electrode exhibits comparatively very low detection limit of CA than other modified electrodes. Thus, $CoFeSe_2$/f-CNF/GCE is a suitable electrode material for sensitive detection of CA.

Selectivity is considered as an essential criteria of electrode material for electrochemical sensor application. In order to observe the selectivity of $CoFeSe_2$/f-CNF/GCE, which was subjected to DPV technique in N_2 saturated 0.05 M PBS (pH 7) with presence of CA (250 μM) and further addition of 50 fold higher concentration of electroactive interferences including catechol (CC), hydroquinone (HQ), epinephrine (EP), dopamine (DA), uric acid (UA) and ascorbic acid (AA) as shown in Fig. 6B. As a result, the addition of interference species is slightly changes the oxidation peak current response of CA. Fig. 6C shows the relative error bar diagram for interference

Table 1
Comparison of the different modified electrode for electrochemical sensing of CA.

Electrode	Technique	LOD (μm)	Linear range (μM)	Ref
eG-quadruplex/hemin	Fluorometry	200	2–350	[37]
AuNPs–chitosan	DPV	25	0.05–2000	[38]
Activated GCE	DPV	68	0.1–1	[39]
Nafion/Tyre/Sonogel-Carbon	Amperometric	60	0.08–2	[40]
Laccase-MWCNT-CS/Au	Amperometric	150	0.7–10	[41]
GCE	DPV	100	10–120	[42]
MIS	DPV	150	0.500–60	[43]
Glassypolymeric carbon	DPV	290	96.5–0.1	[44]
AuNPs/GRNS	DPV	50	0.5–50	[45]
ERGO/Nafion	SWV	90	0.1–10	[46]
GO	DPV	11	0.5–100	[47]
ERGO/SPCE	DPV	0.064	0.2–2100	[25]
Au/PdNPs-GRF	DPV	0.006	0.03–938.97	[48]
NDC/GCE	DPV	0.0024	0.01–350	[49]
$CoFeSe_2$/f-CNF/GCE	DPV	0.002	0.01–263.96	This work

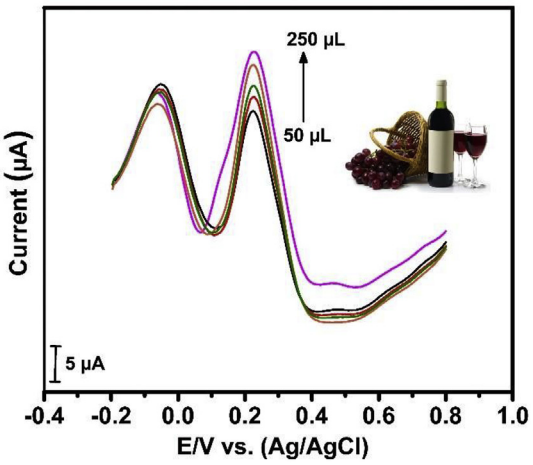

Fig. 7. DPV response for real sample analysis with the addition of wine samples (50–250 µL) in in N_2 saturated PBS (pH 7).

Table 2
Determination of CA in Red wine samples by $CoFeSe_2$/f-CNF/GCE (n = 3).

sample	Found (µM)	RSD (%) (n = 3)
a	99.3	2.1
b	97.1	2.3
c	89.3	2.8

measurement for 100 cycles with the presence of CA (0.196 mM) in N_2 saturated 0.05 M PBS (pH 7) by varying the scan rate of 50 mV s^{-1}. As a result, the fabricated $CoFeSe_2$/f-CNF/GCE exhibits 76.2 % of its initial oxidation peak current of CA even after 100 consequent cycles as shown in Fig. 8A. It implies the unique stability of the reported $CoFeSe_2$/f-CNF/GCE towards the sensing of CA. The five individual $CoFeSe_2$/f-CNF/GCE electrodes were prepared and consequently recorded the CV measurement to investigate the reproducibility as shown in Fig. 8B. As a result, the excellent reproducibility of $CoFeSe_2$/f-CNF/GCE was scrutinized from the resultant RSD value about 2.2 %. Thus, the reported $CoFeSe_2$/f-CNF/GCE exhibits excellent stability and reproducibility during the electrochemical detection of CA.

4. Conclusion

For the first time, $CoFeSe_2$ nanospheres anchored f-CNFs were prepared by facile in-situ hydrothermal synthesis. The developed nanocomposite has been used as an electrode modifier for the electrochemical oxidation of CA. The prepared nanocomposite was systematically characterized by using various analytical techniques which are clearly confirming the formation of $CoFeSe_2$ nanospheres and its anchored on the f-CNFs. In addition, the electrochemical performance of the $CoFeSe_2$/f-CNF/GCE towards redox reaction of CA has been assessed by comparison to bare GCE, $CoFeSe_2$/GCE and f-CNF/GCE. As a result, the $CoFeSe_2$/f-CNF/GCE has been found to show a 10-fold increase in peak current and 0.21 V decrease in overpotential by comparison to bare GCE. Moreover, the well-

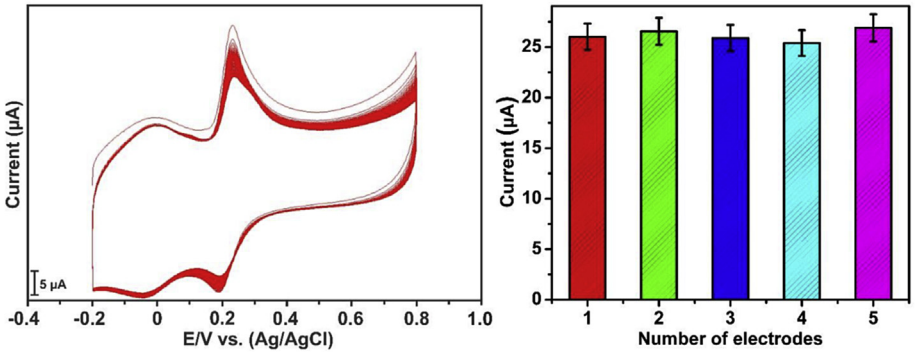

Fig. 8. (A) CV curve for stability with the addition of CA (0.196 mM) in N_2 saturated PBS (pH 7) at a scan rate of 50 mV s^{-1}. Cycle number: 100 consecutive cycles. (B) Bar diagram for reproducibility test.

studies, which shows the percentage value for the variation in oxidation peak current of CA due to the addition of interference species. Hence, the reported $CoFeSe_2$/f-CNF/GCE is a suitable electroactive material for selective determination of CA.

The real-time application of $CoFeSe_2$/f-CNF/GCE was also analyzed by using DPV techniques. For this experiment, three different wine samples were used as the real samples without any pretreatment. Each sample was tested for three times (n = 5). In this experiment, wine samples (50–250 µL) were added directly in N_2 saturated 0.05 M PBS (pH 7). The obtained DPV response is shown in Fig. 7, and the calculated RSD values were presented in Table 2. From this considerable DPV response, $CoFeSe_2$/f-CNF/GCE was found as an efficient electrode material for real-time application.

The stability and reproducibility of fabricated $CoFeSe_2$/f-CNF/GCE are considered as primary criteria for its efficient electrochemical performance towards CA sensing. To understand the stability of $CoFeSe_2$/f-CNF/GCE, which is subjected to continuous CV defined redox behavior of CA is observed at $CoFeSe_2$/f-CNF/GCE with a ΔE_p value of 20 mV which is very lower than that of other modified electrodes. The DPV sensor has shown a linear response in the concentration range from 0.01 to 263.96 µM with a detection limit of 0.002 µM and sensitivity of 2.04 µA μM^{-1} cm^{-2}. Herein, the comparison Table 1 is clearly demonstrating the exclusive improvement and enhanced electrocatalytic activity of the reported $CoFeSe_2$/f-CNF/GCE sensor toward the determination of CA. And also, the excellent anti-interference capability, higher stability and reproducibility of the $CoFeSe_2$/f-CNF/GCE were recorded. Finally, the reported sensor was successfully testified for the detection of CA in real wine sample.

Acknowledgements

Dr. Bose Dinesh gratefully acknowledges DST-SERB for a National Postdoctoral Fellowship (PDF/2015/000174). Financial support of this work by the Ministry of Science and Technology, Taiwan

(NSC101-2113-M-027-001-MY3 to SMC) (MOST 106-2113-M-027-003) is gratefully acknowledged.

Appendix A. Supplementary data

Supplementary data related to this article can be found at https://doi.org/10.1016/j.aca.2017.12.044.

References

[1] S. Mani, S. Ramaraj, S.M. Chen, B. Dinesh, T.W. Chen, Two-dimensional metal chalcogenides analogous $NiSe_2$ nanosheets and its efficient electrocatalytic performance towards glucose sensing, J. Colloid Interface Sci. 507 (2017) 378–385.

[2] Y. Zheng, M. Gao, Q. Gao, H. Li, J. Xu, Z. Wu, S.H. Yu, An efficient $CeO_2/CoSe_2$ nanobelt composite for electrochemical water oxidation, Small 11 (2015) 182–188.

[3] R.J. Toh, C.C.M. Martinez, Z. Sofer, M. Pumera, $MoSe_2$ nanolabels for electrochemical immunoassays, Anal. Chem. 88 (2016) 12204–12209.

[4] L. Mi, H. Sun, Q. Ding, W. Chen, C. Liu, H. Hou, Z. Zheng, C. Shen, 3D hierarchically patterned tubular NiSe with nano-/microstructures for Li ion battery design, Dalton Trans. 41 (2012) 12595.

[5] R.R. Wu, Y. Shi, J. Zhang, B. Zhang, Ni_3Se_2 nanoforest/Nifoam as a hydrophilic, metallic, and self-supported bifunctional electrocatalyst for both H_2 and O_2 generations, Nano Energy 24 (2016) 03–110.

[6] A. Eftekhari, Molybdenum diselenide ($MoSe_2$) for energy storage, catalysis, and optoelectronics, A. Appl. Mater. Today 8 (2017) 1–17.

[7] S.M. Tan, Z. Sofer, J. Luxa, M. Pumera, Aromatic-exfoliated transition metal dichalcogenides: implications for inherent electrochemistry and hydrogen evolution, ACS Catal. 6 (2016) 4594–4607.

[8] Z. Bo, S. Mao, Z.J. Han, K. Cen, J. Chen, K. Ostrikov, Emerging energy and environmental applications of vertically-oriented graphenes, Chem. Soc. Rev. 44 (2015) 2108–2121.

[9] M. Gilic, M. Petrovic, J. Cirkovic, N. Paunovic, S. SavicSevic, Ž. Nikitovic, M. Romcevic, I. Yahia, N. Romcevic, Low-temperature photoluminescence of $CuSe_2$ nano-objects in selenium thin films, Processing Appl. Ceram. 11 (2017) 127–135.

[10] L. Qiao, H.C. Wang, Y. Shen, Y.H. Lin, C.W. Nan, Enhanced photocatalytic performance under visible and near-infrared irradiation of $Cu1.8Se/Cu_3Se_2$ composite via a phase junction, Nanomaterials 7 (2017) 19, https://doi.org/10.3390/nano7010019.

[11] Z. Jin, M. Zhang, M. Wang, C. Feng, Z.S. Wang, Metal selenides as efficient counter electrodes for dye-sensitized solar cells, Acc. Chem. Res. 50 (2017) 895–904.

[12] C.H. Ding, J.J. Tang, S. Chen, Z.Q. Liu, N. Li, Co0.85Se/Multi-Walled carbon nanotube composite as alternative cathode catalyst for microbial fuel cells, J. Nanosci. Nanotechnol. 17 (2017) 1438–1442.

[13] C. Dai, X. Tian, Y. Nie, C. Tian, C. Yang, Z. Zhou, Y. Li, X. Gao, Successful synthesis of 3D $CoSe_2$ hollow microspheres with high surface roughness and its excellent performance in catalytic hydrogen evolution reaction, Chem. Eng. J. (2017), https://doi.org/10.1016/j.cej.2017.03.068.

[14] A. Kumar Dutta, S.K. Maji, A. Mondal, Basudeb Karmakar, P. Biswas, B. Adhikary, Iron selenide thin film: peroxidase-like behavior, glucose detection and amperometric sensing of hydrogen peroxide, Sens. Actuators B 173 (2012) 724–731.

[15] J. Theerthagiri, R. Sudha, K. Premnath, P. Arunachalam, J. Madhavan, A.M. Al-Mayouf, Growth of iron diselenide nanorods on graphene oxide nanosheets as advanced electrocatalyst for hydrogen evolution reaction, Int. J. Hydrogen Energy (2017) 1–11.

[16] H. Xiao, S. Wang, C. Wang, Y. Li, H. Zhang, Z. Wang, Y. Zhou, C. An, J. Zhang, Lamellar structured $CoSe_2$ nanosheets directly arrayed on Ti plate as an efficient electrochemical catalyst for hydrogen evolution, Electrochim. Acta 217 (2016) 156–162.

[17] F. Zhao, S. Shen, L. Cheng, L. Ma, J. Zhou, H. Ye, N. Han, T. Wu, Y. Li, J. Lu, Improved sodium-ion storage performance of ultrasmall iron selenide nanoparticles, Nano Lett. 17 (2017) 4137–4142.

[18] B. Yu, J. Jin, H. Wu, S. Wang, Q. Xia, H. Liu, Iron and nickel doped $CoSe_2$ as efficient non precious metal catalysts for oxygen reduction, Int. J. Hydrogen Energy 42 (2017) 236–242.

[19] N.B. Messaoud, M.E. Ghica, C. Dridi, M.B. Ali, C.M.A. Brett, Electrochemical sensor based on multiwalled carbon nanotube and gold nanoparticle modified electrode for the sensitive detection of bisphenol A, Sens. Actuators, B 253 (2017) 513–522.

[20] Z. Zhao, Y. Wang, P. Li, S. Sang, W. Zhang, J. Hu, K. Lian, A highly sensitive electrochemical sensor based on Cu/Cu_2O@carbon nanocomposite structures for hydrazine detection, Anal. Methods 7 (2015) 9040–9046.

[21] L. Yang, B. Xu, H. Ye, F. Zhao, B. Zeng, A novel quercetin electrochemical sensor based on molecularly imprinted poly (para-aminobenzoic acid) on 3D Pd nanoparticles-porous graphene-carbon nanotubes composite, Sens. Actuators, B 251 (2017) 601–608.

[22] M. Endo, Y.A. Kim, M. Ezaka, K. Osada, T. Yanagisawa, T. Hayashi, M. Terrones, M.S. Dresselhaus, Selective and efficient impregnation of metal nanoparticles on cup-stacked-type carbon nanofibers, Nano Lett. 3 (2003) 6.

[23] Y. Ni, Y. Liao, M. Zheng, and S. Shao, In-situ growth of Co_3O_4 nanoparticles on mesoporous carbon nanofibers: a new nanocomposite for nonenzymatic amperometric sensing of H_2O_2. Microsc. Acta, DOI: https://doi.org/10.1007/s00604-017-2395-9.

[24] J.M.M. Avila, S.S. Valdes, I.Y. Flores, O.S.R. Fernandez, M.G.N. Velazquez, E.H. Hernandez, S.F. Gallardo, F.A. Belmontes, T.L. Ramırez, A.M. Cepeda, P.G. Lafleur, Influence of carbon nanofiber functionalization and compatibilizer on the physical properties of carbon nanofiber reinforced polypropylene nanocomposites, Polym. Compos. (2017), https://doi.org/10.1002/pc.

[25] M. Velmurugan, P. Balasubramanian, S.M. Chen, Determination of caffeic acid in wine samples based on the electrochemical reduction of graphene oxide modified screen printed carbon electrode, Int. J. Electrochem. Sci. 12 (2017) 4173–4182.

[26] R. Karthik, J. Vinoth Kumar, Shen-Ming Chen, P. Senthil Kumar, V. Selvam, and V. Muthuraj, A selective electrochemical sensor for caffeic acid and photocatalyst for metronidazole drug pollutant -A dual role by rod-like SrV_2O_6. Sci. Rep, DOI: https://doi.org/10.1038/s41598-017-07423-1.

[27] J. Li, J. Jiang, M. Liu, Z. Xu, P. Deng, D. Qian, C. Tong, H. Xie, C. Yang, Facile synthesis of MnO_2-embedded flower-like hierarchical porous carbon microspheres as an enhanced electrocatalyst for sensitive detection of caffeic acid, Anal. Chim. Acta 8 (2017) 155–156.

[28] Y.k. zhao, Q.E. Cao, H.T. Liu, K.T. Wang, A.X. Yan, Z.D. Hu, Determination of baicalin, chlorogenic acid, and caffeic acid in traditional Chinese medicinal preparation by capillary zone electrophoresis, Chromotographia 51 (2000) 7–8.

[29] N.B. Cech, M.S. Eleazer, L.T. Shoffner, M.R. Crosswhite, A.C. Davis, A.M. Mortenson, High performance liquid chromatography/electrospray ionization mass spectrometry for simultaneous analysis of alkamides and caffeic acid derivatives from Echinacea purpurea extracts, J. Chromatogr. A 1103 (2006) 219–228.

[30] H. Wang, G.J. Provan, K. Helliwell, Determination of rosmarinic acid and caffeic acid in aromatic herbs by HPLC, Food Chem. 87 (2004) 307–311.

[31] M. Sakthivel, M. Sivakumar, S.M. Chen, Y.S. Hou, V. Veeramani, R. Madhu, N. Miyamoto, A facile synthesis of Cd $(OH)_2$-rGO nanocomposites for the practical electrochemical detection of acetaminophen, Electroanalysis 28 (2016) 1–8.

[32] J.H. Zhan, X.G. Yang, S.D. Li, Y. Xie, W.C. Yu, Y.T. Qian, Synthesis of nanocrystalline cobalt selenide in nonaqueous solvent, J. Solid State Chem. 152 (2000) 537–539.

[33] C. Wei, Y. Bai, A. Deng, Y. Bao, Universal synthesis of air stable, phase pure, controllable $FeSe_2$ nanocrystals, Nanotechnology 27 (2016), 165702.

[34] C.E.M. Campos, J.C. de Lima, T.A. Grandi, K.D. Machado, P.S. Pizani, Structural studies of cobalt selenides prepared by mechanical alloying, Physica B 324 (2002) 409–418.

[35] M. Xiao, Z. Zhang, Y. Tian, Y. Miao, J. Wang, Co-Fe-Se ultrathin nanosheet-fabricated microspheres for efficient electrocatalysis of hydrogen evolution, J. Appl. Electrochem. 47 (2017) 361–367.

[36] M. Sivakumar, M. Sakthivel, S.M. Chen, P. Veerakumar, S.B. Liu, Sol-gel synthesis of carbon-coated $LaCoO_3$ for effective electrocatalytic oxidation of salicylic acid, ChemElectroChem 4 (2017) 1–7.

[37] B. Mancek, S. Kreft, Determination of cichoric acid content in dried press juice of purple coneflower (Echinacea purpurea) with capillary electrophoresis, Talanta 66 (2005) 1094–1097.

[38] E.H. Fernandez, M.G. Romero, A.C. Pancorbo, A.F. Gutierrez, Application and potential of capillary electroseparation methods to determine antioxidant phenolic compounds from plant food material, J Pharm Biomed Anal 53 (2010) 1130–1160.

[39] P. Mattil, J. Hellstrom, J Phenolic acids in potatoes, vegetables, and some of their products, J. J. Food Comp. Anal 20 (2007) 152–160.

[40] A. Hagiwara, M. Hirose, S. Takahashi, K. Ogawa, T. Shirai, N. Ito, Forestomach and kidney carcinogenicity of caffeic acid in F344 rats and C57BL/6NC3H/HeN F1 mice, Cancer Res. 51 (1991) 5655–5660.

[41] H. Fulcrand, A. Cheminat, R. Brouillard, W. Cheynier, Characterization of compounds obtained by chemical oxidation of caffeic acid in acidic conditions, Phytochemistry 35 (1994) 49.

[42] E.N. Sieliwoniuk, J. Nazaruk, E. Antypiuk, A. Kojło, Determination of phenolic compounds and their antioxidant activity in Erigeron acris L. extracts and pharmaceutical formulation by flow injection analysis with inhibited chemiluminescent detection, J Pharm Biomed Anal 48 (2008) 579–586.

[43] Y. Peng, F. Liu, J. Ye, Determination of phenolic acids and flavones in Lonicera japonica thumb. By capillary electrophoresis with electrochemical detection, Electroanalysis 17 (2005) 4.

[44] K. Thangavelu, S. Palanisamy, S.M. Chen, V. Velusamy, T.W. Chen, S.K. Ramaraj, Electrochemical determination of caffeic acid inWine samples using reduced graphene oxide/polydopamine composite, J. Electrochem. Soc. 163 (2016) 726–731.

[45] Y. Zhang, Y. Liu, J. He, P. Pang, Y. Gao, Q. Hu, Electrochemical behavior of caffeic acid assayed with gold nanoparticles/graphene nanosheets modified glassy carbon electrode, Electroanalysis 25 (2013) 1230–1236.

[46] H. Filik, G. Çetintaş, A.A. Avan, S. Aydar, S. NaciKoç, İ. Boz, Square-wave stripping Voltammetric determination of caffeic acid on electrochemically reduced graphene oxide–Nafion composite film, Talanta 116 (2013) 245–250.

[47] M. Meshki, M. Behpour, S. Masoum, Application of multivariate curve

resolution alternating least squares method for determination of caffeic acid in the presence of catechin interference, Anal. Biochem. 473 (2015) 80–88.
[48] T. Kokulnathan, N. Raja, S.M. Chen, W.C. Liao, Nanomolar electrochemical detection of caffeic acid in fortified wine samples based on gold/palladium nanoparticles decorated graphene flakes, J. Colloid Interface Sci. 501 (2017) 77–85.
[49] N. Karikalan, R. Karthik, S. M. Chen, H. A. Chen, A voltammetric determination of caffeic acid in red wines based on the nitrogen doped carbon modified glassy carbon electrode, Sci. Rep, DOI: https://doi.org/10.1038/srep45924.